発表者氏名	論文タイトル	発表誌名	巻 号	ページ	出版年
川島素子，山田昌和，河合正孝，篠田啓，仁科幸子	癒着性斜視に対する羊膜移植，自己結膜移植，ゼラチンスポンジ挿入術	眼科手術	17巻3号	409-413	2004
井上真、永井紀博、野田航介、今村裕、石田晋、篠田啓、小口芳久	黄斑前膜に対する minimal vitrectomy	眼科	46	449-453	2004
内田敦郎，井上真，篠田肇，篠田啓，黒坂大次郎，桂弘	後嚢破損を生じたアトピー白内障の予後	日本眼科紀要	55巻12号	949-952	2004
永井紀博，木村至，大出尚郎，篠田啓，北和典，真島行彦，小口芳久	Multifocal Visual Evoked Potentials による両眼加算の解析	日本眼科紀要	55巻9号	711-714	2004
Tatar O, Adam A, Shinoda K, Stalmans P, Eckardt C, Lüke M, Bartz-Schmidt KU, Grisanti S	Expression of VEGF and PEDF in choroidal neovascular membranes following verteporfin photodynamic therapy	Am J Ophthalmol.		In press.	
Sugisaka E, Shinoda K, Ishida S, Imamura Y, Ozawa Y, Nakajima T, Shinoda H, Suzuki K, Kawaguchi N, Inoue M.	Visual Sensations during Pars Plana Vitrectomy under Retrobulbar Anesthesia	Ophthalmology		In press	
Tatar O, Shinoda K, Adam A, Rohrbach JM, Lucke K, Henke-Fahle S, Bartz-Schmidt KU, Grisanti S	Expression of Endostatin in human choroidal neovascular membranes secondary to age-related macular degeneration	Exp Eye Res		In press	
Tatar O, Kaiserling E, Adam A, Gelisken F, Shinoda K, Völker M, Lafaut BA, Bartz-Schmidt KU, Grisanti S	Consequences of verteporfin photodynamic therapy on choroidal neovascular membranes	Arch Ophthalmol		In press	
Yamaguchi T, Inoue M, Ishida S, Shinoda K	Detecting Vitreomacular Adhesions in Eyes with Asteroid Hyalosis with Triamcinolone Acetonide	Graefes Arch Clin Exp Ophthalmol	13	1-4	2006
Sato EA, Ohtake Y, Shinoda K, Mashima Y, Kimura I	Decreased Blood Flow at Neuroretinal Rim of Optic Nerve Head Corresponds with Visual Field Deficit in Eyes with Normal Tension Glaucoma	Graefes Arch Clin Exp Ophthalmol	29	1-7	2005
Yokoyama S, Kimura I, Ohde H, Shinoda K, Mashima Y	Microcirculation at Optic Disc Rim is Correlated with Visual Field Defects in Cases of Anterior Ischemic Optic Neuropathy	Clin Exp Ophthalmol		In press	

発表者氏名	論文タイトル	発表誌名	巻 号	ページ	出版年
Kawaguchi N, Inoue M, Sugisaka E, Shinoda K, Tsubota K	Subjective Visual Sensation during Vitrectomy under Retrobulbar Anesthesia	Am J Ophthalmol	141 (2)	407-9	2006
Schuettauf F, Eibl KH, Thaler S, Shinoda K, Rejdak R, May CA, Blatsios G, Welge-Lussen U	Toxicity study of erucylphosphocholine in a rat model	Curr Eye Res	30 (9)	813-20	2005
Inoue M, Shinoda K, Ishida S, Uchida A, Kurosaka D, Katsura H, Tsubota K	Intraocular Lens Implantation after Atopic Cataract Surgery Decreases Incidence of Postoperative Retinal Detachment	Ophthalmology	9	Epub ahead of print	2005
Gekeler F, Shinoda K, Blatsios G, Werner A, Zrenner E	Scotopic threshold responses to infrared irradiation in cats	Vision Res	1	Epub ahead of print	2005
Satofuka S, Inoue M, Shinoda K, Ishida S, Imamura Y, Ando Y	Adherence of intravitreally injected triamcinolone acetonide to the denuded retinal surface after internal limiting membrane peeling	Retina	25 (5)	672-3	2005
Kimura I, Shinoda K, Tanino T, Ohtake Y, Mashima Y	Effect of topical unoprostone isopropyl on optic nerve head circulation in controls and in normal-tension glaucoma patients	Jpn J Ophthalmol	49 (4)	287-93	2005
Nagai N, Oike Y, Noda K, Urano T, Kubota Y, Ozawa Y, Shinoda H, Koto T, Shinoda K, Inoue M, Tsubota K, Yamashiro K, Suda T, Ishida S	Suppression of Ocular Inflammation in Endotoxin-Induced Uveitis by Blocking the Angiotensin II Type 1 Receptor	Invest Ophthalmol Vis Sci	46 (8)	2925-31	2005
Okuda A, Inoue M, Shinoda K, Tsubota K	Massive bilateral vitreoretinal hemorrhage in patient with chronic refractory idiopathic thrombocytopenic purpura	Graefes Arch Clin Exp Ophthalmol		Epub ahead of print	2005
井上真, 篠田啓	25 ゲージ硝子体手術システムのまとめ	眼科手術	18 (3)	373-377	2005
Terauchi N, Fujinami K, Shinoda K, Tsunoda K, Hanazono G, Inomata K, Miyake Y	Transient macular ischemia determined by focal macular electroretinogram	Br J Ophthalmol.		In press	

発表者氏名	論文タイトル	発表誌名	巻 号	ページ	出版年
Hanazono G, Tsunoda K, Shinoda K, Tanifuji M, Miyake Y	Intrinsic Signal Imaging in Macaque's Retina Reveals Different Types of Flash-induced Light Reflectance Changes of Different Origins	Invest Ophthalmol Vis Sci.		In press	
Ban Y, Shinoda K, Ohde H, Kaneda E	Enlargement of Optic Nerve Resembling Orbital Mass in Case of Optic Neuritis	Graefes Arch Clin Exp Ophthalmol		Epub ahead of print	2007
Sailer H, Shinoda K, Blatsios, Kohler K, Bondzio L, Zrenner E, Gekeler F	Investigation of thermal effects of infrared lasers on the rabbit retina: a study in the course of the development of an active subretinal prosthesis	Graefes Arch Clin Exp Ophthalmol		Epub ahead of print	2007
Sato EA, Shinoda K, Kimura I, Ohtake Y, Inoue M	Microcirculation in Eyes after Rhegmatogenous Retinal Detachment Surgery	Curr Eye Res		In press	
Sato EA, Inoue M, Kimura I, Ohtake Y, Shinoda K	Reduced Chroidal Blood Flow can Induce Visual Field Defect in Open Angle Glaucoma Patients without Intraocular Pressure Elevation following Encircling Scleral Buckling	RETINA		In press	
Watanabe K, Shinoda K, Kimura I, Mashima Y, Ohde H	Dissociation of Conventional Visual field Tests and Multifocal Visual Evoked Potentials in Patients with Hemianopsia	Am J Ophthalmol		Epub ahead of print	2006
Chen CJ, Satofuka S, Inoue M, Ishida S, Shinoda K, Imamura Y, Tsubota K	Suprachoroidal hemorrhage caused by breakage of 25-gauge cannula	Ophthalmic Laser Surgery Imaging 2006		In press	2006
Kimura I, Shinoda K, Eshita T, Inoue M, Mashima Y	Relaxation of encircling buckle improved choroidal blood flow in a patient with visual field defect following encircling procedure	Jpn J Ophthalmol	50 (6)	554-556	2006
Kurihata T, Ozawa Y, Shinoda K, Nagai N, Inoue M, Oike Y, Tsubota K, Ishida S, Okano H	Neuroprotective effects of angiotensin II type 1 receptor (AT1R) blocker, telmisartan via modulating AT1R and AT2R signaling in retinal inflammation	Invest Ophthalmol Vis Sci.	47 (12)	5545-5552	2006

発表者氏名	論文タイトル	発表誌名	巻 号	ページ	出版年
Gekeler F, Shinoda K, Jünger M, Bartz-Schmidt KU, Gelisken F	Three cases of familial Retinal Arterial//Tortuosity//(fRAT) associated with tortuosity of capillaries in nailfold capillaroscopy as an indication for a systemic disease	Arch Ophthalmol	124 (10)	1492-1494	2006
Inoue M, Shinoda K, Ohde H, Tezuka K, Hida T	Phototoxic effects of commerc ial photographic flash lamp on rat eyes	Doc Ophthalmol	113 (3)	155-164	2006
Imamura Y, Noda S, Hashizume K, Shinoda K, Yamaguchi M, Uchiyama S, Shimizu T, Mizushima Y, Shirasawa T, Tsubota K	Drusen, choroidal neovasculari zation, and retinal pigment epithelium dysfunction in SOD1-deficient mice: A model of//age-related macular degeneration	Proc Natl Acad Sci U S A	103 (30)	11282-11287	2006
Yokoyama S, Kimura I, OhdeH, Shinoda K, Mashima Y	Microcirculation at Optic Disc Rim is Correlated with Visual Field Defects in Cases of Anterior Ischemic Optic Neuropathy	Clin Exp Ophthalmol	34 (5)	491-493	2006
Tatar O, Adam A, Shinoda K, Stalmans P, Eckardt C, Lüke M, Bartz-Schmidt KU, Grisanti S	Expression of VEGF and PEDF in Choroidal Neovascular Membranes Following Verteporfin Photodynamic Therapy	Am J Ophthalmol.	142 (1)	95-104	2006
Sugisaka E, Shinoda K, Ishida S, Imamura Y, Ozawa Y, Nakajima T, Shinoda H, Suzuki//K, Kawaguchi N, Inoue M	Visual Sensations during Pars Plana Vitrectomy under Retrobulbar Anesthesia	Ophthalmology.	113 (10)	1886	2006
Eckhorn R, Wilms M, Schanze T, Eger M, Hesse L, Eysel UT, Kisvarday ZF, Zrenner E, Gekeler F, Schwahn H, Shinoda K, Sachs H, Walter P	Visual resolution with retinal implants estimated from recordings in cat visual cortex	Vision Res	46 (17)	2675-2690	2006
Tatar O, Shinoda K, Adam A, Rohrbach JM, Lucke K, Henke-Fahle S, Bartz-Sch midt KU, Grisanti S	Expression of Endostatin in human choroidal neovascular membranes secondary to age-r elated macular degeneration	Exp Eye Res	83 (2)	329-338	2006

発表者氏名	論文タイトル	発表誌名	巻 号	ページ	出版年
Tatar O, Kaiserling E, Adam A, Gelisken F, Shinoda K, Völker M, Lafaut BA, Bartz-Schmidt KU, Grisanti S	Consequences of verteporfin photodynamic therapy on chor oidal neovascular membranes	Arch Ophthalmol	124 (6)	815-823	2006
篠田啓	人工網膜の開発-世界の現況	日本の眼科	77	651-654	2006
篠田啓	X連鎖若年網膜分離症	眼科	48	1661-1668	2006

Ⅲ. 研究成果の刊行物・別刷

Mapping Cone- and Rod-Induced Retinal Responsiveness in Macaque Retina by Optical Imaging

Kazushige Tsunoda,[1,2] *Yoshihisa Oguchi,*[3] *Gen Hanazono,*[3] *and Manabu Tanifuji*[1]

Mapping Cone- and Rod-Induced Retinal Responsiveness in Macaque Retina by Optical Imaging

Kazushige Tsunoda,[1,2] *Yoshihisa Oguchi,*[3] *Gen Hanazono,*[3] *and Manabu Tanifuji*[1]

Purpose. To map the distribution of cone- or rod-induced retinal responsiveness by optical imaging from macaque retina.

Methods. The light reflectance changes in the posterior retina after a flash stimulus in anesthetized rhesus monkeys were measured by a modified fundus camera system equipped with a charge-coupled device (CCD) camera. The response topography of the optical signals was obtained in either light- or dark-adapted conditions.

Results. With infrared observation light, the whole posterior pole became darkened after the stimulus. The response topography in light-adapted conditions demonstrated a steep peak of darkening at the fovea, together with the gradual decrease of signal intensity away from the fovea toward the periphery. In dark-adapted conditions, the optical signal showed additional peaks along the circular region surrounding the macula at the eccentricity of the optic disc, together with the central peak at the fovea. A statistically significant positive correlation was obtained between the light reflectance changes in infrared observation light and the focal responses in multifocal electroretinogram (mfERG) at the corresponding retinal locations.

Conclusions. The response topography in the retina, obtained by optical imaging, was consistent with psychophysical cone or rod sensitivity in humans and anatomic cone or rod distribution in humans and macaques. The cone- or rod-induced retinal responsiveness within the posterior pole region was noninvasively recorded within a short recording time. (*Invest Ophthalmol Vis Sci.* 2004;45:3820–3826) DOI:10.1167/iovs.04-0394

Since the early pioneering work by Osterberg,[1] there have been numerous reports about the detailed anatomic distribution of photoreceptors in monkey or human retina,[2–4] and recently, the mosaic arrangement of three types of cones has been precisely analyzed, even in living subjects.[5] Because visual acuity or size of visual field depends not only on the anatomic density but more on the neural function of photoreceptors, mapping retinal responsiveness is important from both physiological and clinical points of view. However, detailed response topography of cone and rod photoreceptors have not been revealed with the current capabilities of the conventional objective measurements, such as the multifocal electroretinogram (mfERG),[6–8] flicker-evoked flowmetry,[9] and functional MRI (fMRI).[10]

Optical imaging based on intrinsic signals is a well-established imaging technique for visualizing neural activity. Since Blasdel and Salama[11] and Grinvald et al.[12] successfully visualized in living animals the functional organization of the primary visual cortex, such as the orientation column and ocular dominance column, this technique has been widely used in the past decade to map the functional organization of the various areas of the visual cortex,[13] such as V1,[14,15] V2,[16] V4,[17] MT,[18] and TE.[19] In optical imaging, the decrease in light reflectance elicited by neural activation is measured from the cortical surface by a charge-coupled device (CCD) camera, without using extrinsic probes. The reflectance changes are due to multiple metabolic changes after neural activation. For example, the optical signal measured at ~540 nm is dominated by blood volume changes in capillaries, that, at 600 to 650 nm, is dominated by the change in deoxygenation level of hemoglobin and that, in infrared light, is dominated by the change in tissue light-scattering.[20] Although different metabolic changes are emphasized at different wavelengths, optical responses obtained at these wavelengths give nearly the same spatial pattern that corresponds to the spatial pattern of activated neurons.[15,21]

The optical imaging technique with intrinsic signals has advantages over other functional neuroimaging techniques, such as positron emission tomography,[22,23] fMRI,[24–26] and near-infrared optical topography,[27,28] in that the spatial resolution is as good as 50 μm and the time resolution is less than 1 second. Although the reflectance change is not a direct measure of neural activation, the intrinsic signals coincide well with the activity of neurons examined by conventional extracellular recordings,[19,29,30] and the mass responses of clusters of neurons can be easily mapped simultaneously from large area of the cortex. Measuring intrinsic signals, however, requires surgical exposure of the cortical surface, and an optical chamber should be mounted on the skull to clear the cortical view and reduce the cortical movements induced by heartbeat and respiration. Thus, its application to clinical examination is severely limited.[31,32] The eyeball with transparent ocular media, on the contrary, works as an ideal optical chamber through which retinal reflectance changes can be clearly and stably monitored without any surgical invasion, and the optical imaging is likely to be of considerable value in ocular examination.

Previous studies, measuring light reflection from in vivo retina, mainly focused on the anatomic distribution of cone photopigment,[33,34] macular pigment,[35,36] and cone mosaic,[5] and few of them directly dealt with light reflectance changes related to neural activities.

In the current study, we applied the technique of optical imaging to macaque retina and, for the first time, successfully demonstrated the stimulus-evoked response topography that reflects cone- and rod-induced photoreceptor function. The purpose of this study was to investigate the basic properties of intrinsic signals in macaque retina, for the future establishment of a new diagnostic system by which early detection of functional disorders in retina, such as age-related macular degener-

From the [1]Laboratory for Integrative Neural Systems, Riken Brain Science Institute, Saitama, Japan; the [2]Laboratory of Visual Physiology, National Institute of Sensory Organs, Tokyo, Japan; and the [3]Department of Ophthalmology, Keio University School of Medicine, Tokyo, Japan.

Submitted for publication April 7, 2004; revised June 22, 2004; accepted June 29, 2004.

Disclosure: **K. Tsunoda**, None; **Y. Oguchi**, None; **G. Hanazono**, None; **M. Tanifuji**, None

The publication costs of this article were defrayed in part by page charge payment. This article must therefore be marked "*advertisement*" in accordance with 18 U.S.C. §1734 solely to indicate this fact.

Corresponding author: Kazushige Tsunoda, Laboratory for Integrative Neural Systems, Riken Brain Science Institute, 2-1 Hirosawa, Wako-shi, Saitama 351-0198, Japan; tsunoda@postman.riken.jp.

Investigative Ophthalmology & Visual Science, October 2004, Vol. 45, No. 10

ation (ARMD), retinitis pigmentosa, and various retinal diseases in infants, can be made noninvasively.

METHODS

The experiments were performed on two Rhesus monkeys (*Macaca mulatta*) (denoted M1 and M2) under anesthesia. After intramuscular injection of atropine sulfate (0.08 mg/kg), droperidol (0.25 mg/kg), and ketamine (5.0 mg/kg), the monkeys were paralyzed with vecuronium bromide (0.2 mg/kg per hour) and artificially ventilated with a mixture of N_2O, O_2, and isoflurane (70% N_2O, 30% O_2, isoflurane up to 2.0%). Electroencephalogram and electrocardiogram, expired CO_2 concentration, and rectal temperature were monitored throughout the experiments. Before recordings were made, the pupil was fully dilated with topical tropicamide (0.5%) and phenylephrine hydrochloride (0.5%), and eye movements were completely blocked with an additional dose of vecuronium bromide. The experimental protocol was approved by the Experimental Animal Committee of the Riken Institute. All experimental procedures were performed in accordance with the guidelines of the Riken Institute and the ARVO Statement for the Use of Animals in Ophthalmic and Vision Research.

Optical Imaging and Data Analysis

We modified a digital fundus camera system (NM-1000; Nidek, Aichi, Japan) to measure the light reflectance changes from the ocular fundus. Fundus images were obtained using a CCD camera (PX-30BC; Primetech Engineering, Tokyo, Japan) and digitized with an IBM compatible computer, equipped with a video frame-grabber board (Pulsar; Matrox, Quebec, Canada: gray-level resolution, 10 bit; spatial resolution, 640 × 480; temporal resolution, 1/30 second; Fig. 1A). The recording area covered 45°, including the macula, superior and inferior vascular arcades, and optic disc, and the image was focused at the surface of macular vessels. Throughout the recording of a trial, the posterior fundus was continuously illuminated with light from a halogen lamp (observation light), which passed through one of the bandpass interference filters: 650 and 900 nm, with 30 and 120-nm bandwidths, respectively. Each recording trial took 8 seconds and consisted of 16 consecutive averaged images, each of which consisted of 15 gray-scale video frames (Fig. 1B). A white Xenon flash stimulus (duration: 1 ms) was given to the whole posterior region of the ocular fundus, 1250 ms after the initiation of data acquisition. The flash intensity measured in front of the eye was 41.9 cd-s/m^2. The timing of data acquisition and stimulus delivery was under computer control.

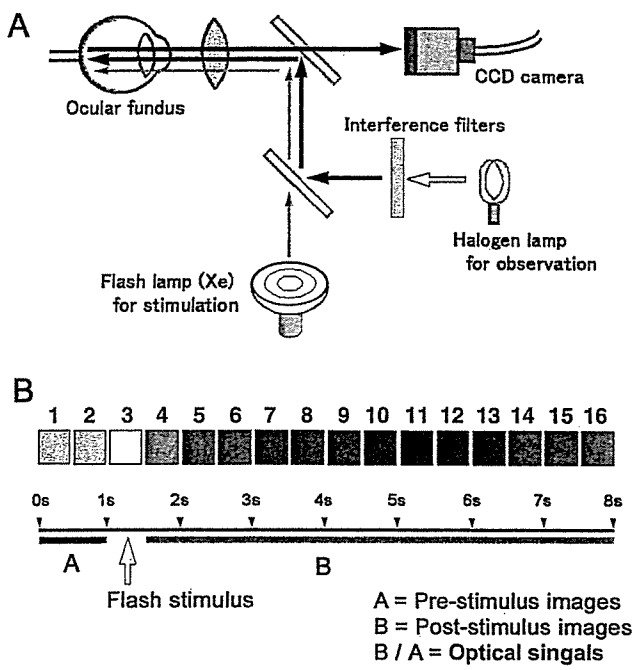

FIGURE 1. (A) Schematic drawing of the experimental setup. Throughout the recording trial, the fundus was continuously illuminated with observation light through one of the bandpass filters. (B) The recording protocol of one trial lasting 8 seconds (16 images). Before stimulus delivery, prestimulus images were taken to make a reference image of baseline light reflectance. Flash stimulus was administered in the middle of the third image. Each of the 16 consecutive boxes shows an averaged fundus image, containing 15 video frames taken across 500 ms.

Changes in light reflectance from the ocular fundus (optical signals), such as darkening (decrease in light reflectance) and brightening (increase in light reflectance) of the retina, were observed after flash stimulus. The optical signal was calculated as follows[19]: (1) Each image size was reduced to 320 × 240 pixels by 2 × 2 binning, and (2) the gray-scale values of the images obtained after stimulus were divided, pixel by pixel, by those obtained during a 1-second period before the stimulus. This ratio was rescaled to 256 levels of gray-scale resolution to show the stimulus-driven reflectance changes. Recording trials with severe motion artifacts or large physiological noise were excluded from the analysis.

Two-dimensional images of the optical signals were obtained from a single trial without averaging data from different trials (Fig. 2A). In the recording sessions to measure the signal time course, 8-second trials were consecutively run 20 times in monkey M1, with 10-minute intervals between flashes under dark condition. Among them, five trials with a high noise level were excluded. The result of 15 trials is shown in Figure 2B. In the recording sessions to map the response topography, each trial was consecutively performed after 15 (light-adapted condition) or 40 (dark-adapted condition) minutes' adaptation (Figs. 3A, 4A). The eye was light adapted by a Ganzfeld bowl with a background luminance of 30 cd/m^2. Basically, the result of a single trial could show a typical response topography. However, to obtain the response topography shown in Figures 3 and 4, three consecutive trials were averaged to reduce the "shot noise" derived from the observation light itself. To make a three-dimensional topographic map of signal intensity, a median filter (6 × 6 pixels) was applied (Figs. 3B, 4B).

In retinal optical imaging, there are two important issues in choosing the wavelength of observation light: (1) During the whole period of recording, the retina is continuously illuminated with the observation light to measure the reflectance changes. If visible light is used for observation, it evokes neural activities, and the reflectance can be changed without giving flash stimulus. The baseline retinal reflectance thus becomes unstable and unsuitable for evaluating the retinal response. For example, visible observation light at a wavelength of 650 nm could elicit changes in light reflectance without flash stimulus, and even after 10 minutes of adaptation to the observation light, the reflectance change of −0.08% was observed during the recording period of 8 seconds (Fig. 2B, left panel, no flash). Under infrared light (900 nm), however, the fluctuation of light reflectance was as little as −0.02% (Fig. 2B, right panel, no flash). (2) It is well known that after bleaching of photopigments, the macular reflectance for visible light illumination is dramatically increased (retinal image looks brighter; Fig. 2A, 650 nm) and this phenomenon could be very useful for functional evaluation of the macula. The problem is that the bleaching-related reflectance change has a polarity opposite to the reflectance change that is caused by tissue light-scattering and hemoglobin concentration changes, which are commonly observed as decreases in light reflectance (the retinal image looks darker; Fig. 2A, infrared). Considering that imaging with visible light is composed of multiple signal components with different polarities, the data of optical imaging under visible observation light is not useful for mapping retinal responses. Therefore, the observation light used in our study should have negligible absorption by the photopigments,[37] and this would allow a correct mapping of the stimulus-evoked response topography. In the present study, data with 650 nm light were also presented, representing re-

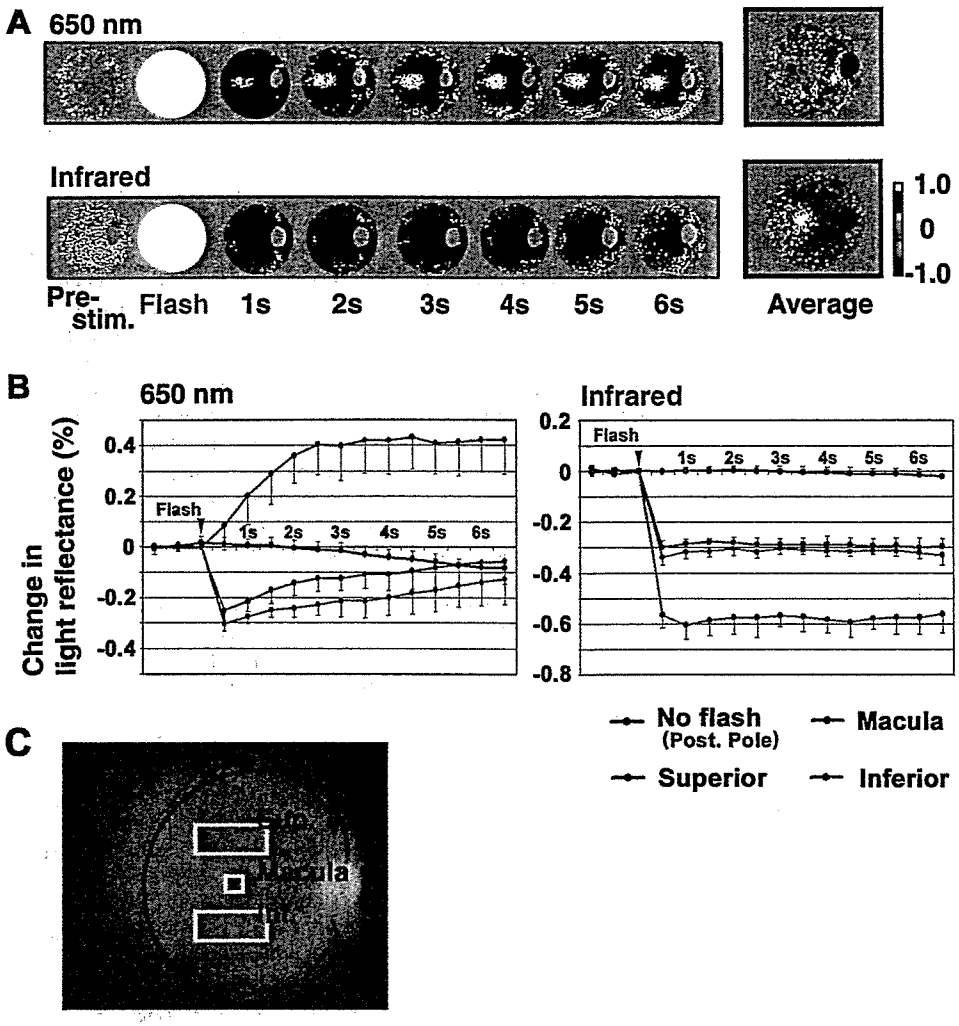

FIGURE 2. (A) Time courses of two-dimensional images of retina showing light reflectance changes after a flash stimulus observed with 650 nm and infrared light (900 nm), measured in the posterior pole region of normal retina in (C). The images in the second column were saturated by the strong reflection of the flash stimulus. The averaged reflectance changes during initial 3 seconds after stimulus are shown in pseudocolor maps on the *right*, with landmarks such as retinal vessels and the optic disc indicated in *black*. Color indicates relative light reflectance decrease (darkening) from prestimulus level. (B) Time courses of light reflectance changes, with or without stimulus under observation light at 650 and 900 nm (infrared) at various regions in a normal eye. The data were averaged among 15 trials. Spontaneous reflectance changes (no flash) in the posterior pole region, and stimulus evoked reflectance changes in superior, inferior, and macular regions were plotted as averaged reflectances ± SD within the corresponding local regions in (C). (C) Fundus photograph of a normal retina, indicating the recording areas. Sup., superior posterior pole; Inf., inferior posterior pole.

cording with visible light, because red observation light (600–700 nm) is most commonly used in brain optical imaging.

Multifocal Electroretinogram

mfERG measures the local retinal activity in multiple small regions in the posterior retina by presenting on a television monitor an achromatic flicker that alternates independently between black and white in individual hexagonal segments.[7,8,38] Multifocal ERGs were recorded and analyzed with a visual evoked response imaging system (VERIS; EDI, San Mateo, CA) with a Burian-Allen bipolar contact lens electrode. Foveal position was adjusted by projecting the retinal image onto the monitor through a modified retinoscope. The luminance of each hexagon was 200 cd/m^2 (white) or 10 cd/m^2 (black), with the surround at 100 cd/m^2. Thirty-seven equally sized hexagonal elements (each 3.6° wide) were displayed at a 75-Hz frame rate, and recordings were collected in either the normal or artificially damaged eye of monkey M1, with 4 minutes' total duration. Amplitudes of the focal first-order responses were estimated by a scalar product method.[7] The correlation between the amplitude of the local mfERGs and the magnitude of the local reflectance changes was calculated. For this, the fundus was divided into 15 separate regions. Three optical measurements taken on separate days were compared with one mfERG (Figs. 3C, 3D, 5C, 5D).

Argon Laser Photocoagulation

To reduce the function of outer retina artificially, the left fundus in M1 was locally coagulated with argon laser photocoagulation (ALC; wavelength: 514 nm, spot size: 500 μm, power: 160 mW).[39] As many as 1500 spots were densely scattered in the top half of the retina within the equator, so that the distance between each spot was as close as 100 μm (Fig. 5). The optical imaging and mfERG were conducted 1 month after ALC, when the ALC spots had formed complete scars, and no macular edema was observed, either by fluorescein angiography or funduscopic examination.

RESULTS

With observation light having a wavelength of 650 nm, the light reflectance from the macula increased (retinal image became brighter), whereas the light reflectance from the posterior pole region apart from the macula decreased (retinal image became darkener) after a flash stimulus (Fig. 2A). The time course of light reflectance changes in the macular region was quite different from that in perimacular regions (Fig. 2B). The increase in light reflectance after a flash in the macular region is attributable to the bleaching of photopigments by visible light.[33,34,37,40] In contrast, the decrease in light reflectance in the perimacular region is attributable to the hemoglobin-related reflectance changes or tissue light-scattering changes that are observed in the cerebral cortex.[20]

With infrared observation light, the whole posterior region became darker for at least 6 seconds after the stimulus, and the pseudocolor map shows that there was a peak of light reflectance decrease at the center (Fig. 2A). The signal time course shows that the light reflectance from the retina decreased after the flash stimulus and reached its peak no later than 1 second after stimulus onset (Fig. 2B). The response topography in the

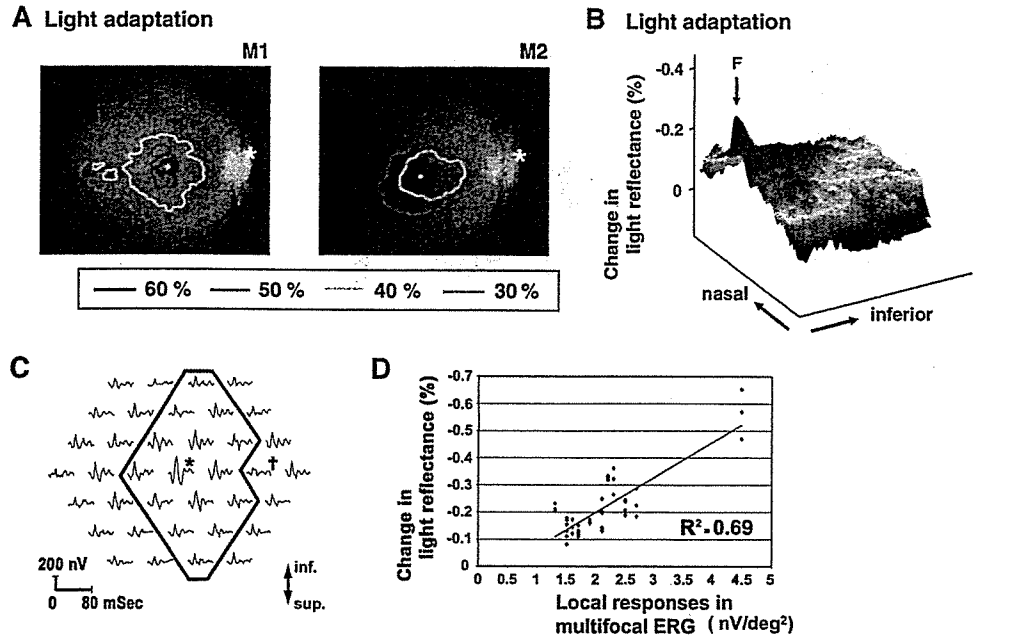

FIGURE 3. (A) Response topography of normal retina in light-adapted conditions in two monkeys (M1 and M2). *White dot*: foveal center; *asterisk*: optic disc. Regions with 60%, 50%, 40%, and 30% of the peak signal intensity at the fovea are outlined by different colors. (B) Pseudocolor topographic maps of light reflectance changes in the inferior retina, profiled along the horizontal meridian, in the light-adapted condition. Three consecutive trials were averaged to make up the topographic map in M1 (same in Fig. 4). The location of the fovea is indicated by F (*arrow*). (C) Array of 37 local mfERG responses in normal retina. The responses of 15 elements (inside the frame) were taken for correlation analysis. ERGs with * and † indicate the location of macula and optic disc, respectively. (D) Correlation between the optical signal (decrease in light reflectance) obtained with 900 nm illumination and the scalar product of the first-order kernel of the mfERG from the corresponding retinal locations ($R^2 = 0.69$, $P < 0.001$, $n = 45$). To emphasize the negative peak, we used graphic scaling opposite to convention.

light-adapted condition demonstrated a steep peak of darkening at the fovea, together with the gradual decrease of signal intensity away from the fovea toward the periphery (Figs. 3A, 3B). This is consistent with the topography of psychophysical cone sensitivity in normal human subjects measured with bright background.[41,42] To make sure that the central peak of darkening reflected the cone-related retinal response, the local optical signal values in the light-adapted condition were compared with the local neuronal activities, measured electrophysiologically by mfERG, that are thought to reflect the cone-mediated retinal activity (Figs. 3C, 3D).[7,38] We found a statistically significant correlation between the light reflec-

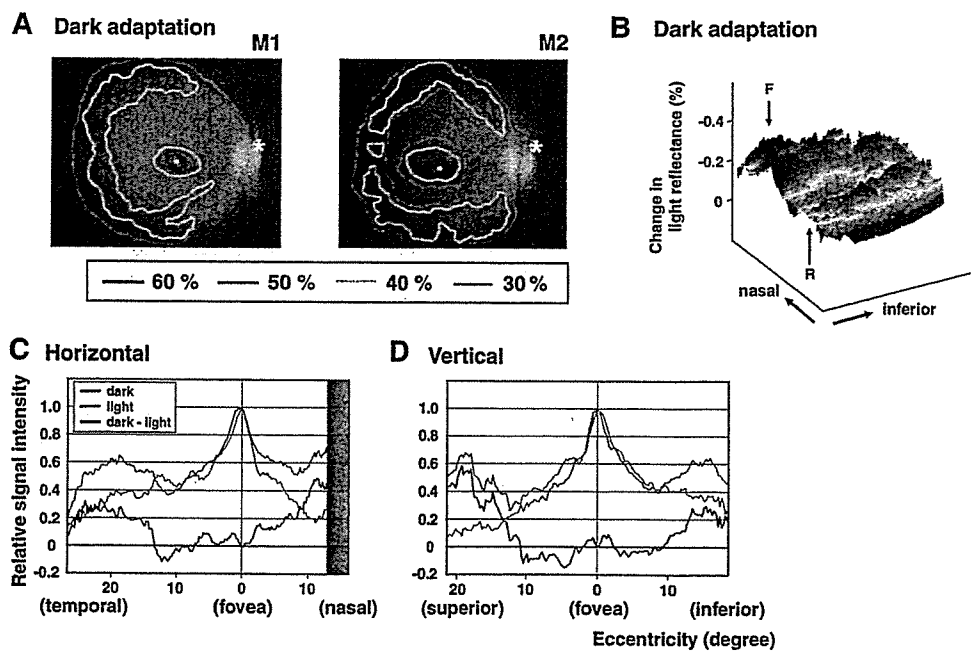

FIGURE 4. (A) Response topography of normal retina under dark-adapted conditions. (B) Pseudocolor topographic maps of light reflectance changes in the inferior retina, profiled along the horizontal meridian, under dark-adapted conditions. F: the fovea; R: crest of the rod ring. (C, D) Signal-intensity profiles along the horizontal (C) and vertical (D) meridians as a function of eccentricity from the foveal center, under dark- and light-adapted conditions. The signal intensity was averaged among three consecutive trials in monkey M1. The peak intensities at the fovea were normalized to 1.0 in both conditions. *Black traces*: estimated rod-induced relative response profiles. The *red* region on the *x*-axis corresponds to the optic disc in the nasal retina.

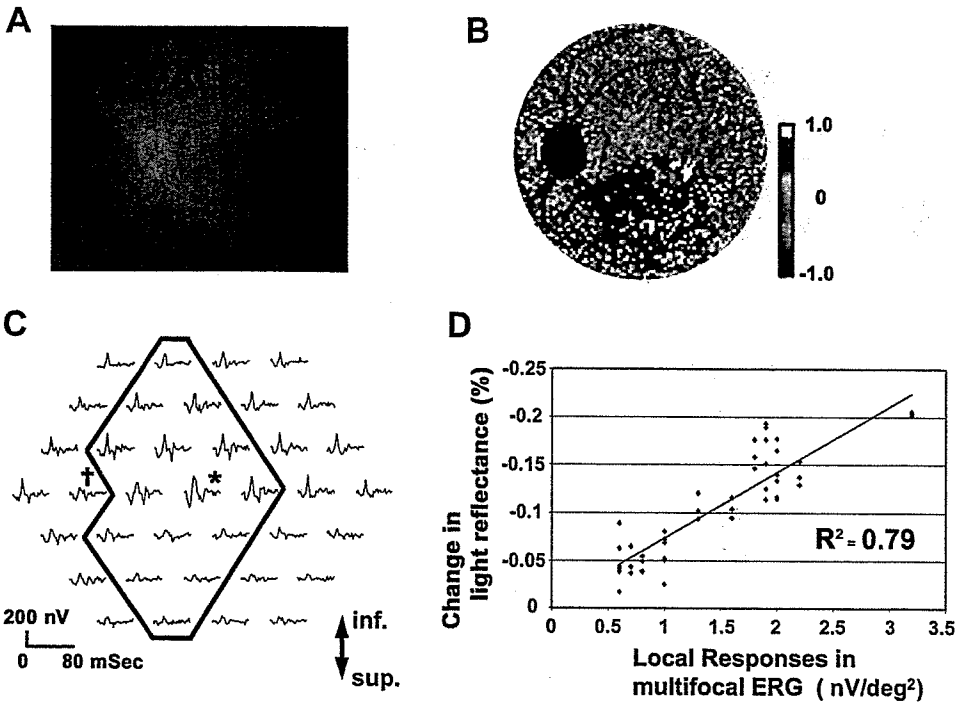

FIGURE 5. (A) Fundus photograph of the artificially damaged eye. The top half of the posterior retina was densely coagulated with ALC, sparing the macular area. (B) Pseudocolor map of optical signals averaged over the initial 3 seconds under infrared light. Color indicates relative light reflectance decrease (darkening) from prestimulus level. (C) Array of 37 local responses of mfERG, taken from the fundus in (A). ERGs with * and † indicate the location of macula and optic disc, respectively. (D) Correlation between the optical signal (decrease in light reflectance) obtained with 900 nm illumination and the scalar product of the first-order kernel of the mfERG from the corresponding retinal locations ($R^2 = 0.79$, $P < 0.001$, $n = 45$).

tance change under infrared observation light and the focal responses in mfERG at the corresponding sites in normal retina ($R^2 = 0.69$, $P < 0.001$, $n = 45$), indicating that the topography of optical signal response reflects cone-related retinal function.

If the optical signal reflects the central accumulation of photoreceptors in the light-adapted condition, the local retinal region, which is called rod ring with high rod density, should also be activated in the dark-adapted condition.[3,4] After 40 minutes of dark adaptation, the optical signal showed additional peaks along the circular region surrounding the macula at the eccentricity of the optic disc, together with a central peak at the fovea (Figs. 4A, 4B). By assuming that the optical signals measured under light-adapted condition reflect only the cone-induced response, we estimated the relative response profile of rods by subtracting the signal in the light-adapted condition from that in the dark-adapted condition. The optical signal amplitudes of the cone-induced central peak were almost the same in dark- and light-adapted conditions (data not shown). The averaged signal intensity along the horizontal and vertical meridian in three recording trials was plotted as a signal intensity profile relative to the peak value (Figs. 4C, 4D). The profiles along the horizontal and vertical meridians showed that the estimated rod response had peaks at 22.0° in temporal, 18.5° in superior, and 15.0° in inferior retina from the foveal center. These peak eccentricities were consistent with the location of peak in psychophysical rod sensitivity in normal human subjects.[43,44] The response peak at the nasal retina was not measurable because of the presence of the optic disc.

To see whether optical imaging could map the area with a functional lesion, we used ALC for local coagulation of the left fundus in M1 (Fig. 5A). One month after the procedure, the structure of the outer retina, including photoreceptors and pigment epithelial cells, was thought to be widely damaged,[39] and the electrophysiological responses in the damaged region were reduced accordingly (Fig. 5C). Similar to the data from the normal eye, the light reflectance decrease and the mfERG signal showed statistically significant correlation in the eye artificially damaged by ALC ($R^2 = 0.79$, $P < 0.001$, $n = 45$). The results of optical imaging and electrophysiological measurement were well correlated not only in their response amplitudes but also in the spatial location of reduced responses: the border between normal and reduced response regions in both measurements corresponded to the border between the normal site and the area of photocoagulation (Figs. 5A–C).

DISCUSSION

Local neural activity induces various metabolic changes, and some of them cause changes in light reflectance from tissue. For example, neural activation elicits increases in deoxygenated hemoglobin concentration and in tissue blood volume. Intrinsic signals in cerebral cortex, stimulus-induced light reflectance changes, partly originate from light absorption changes due to these hemoglobin concentration changes.[20,21] Neural activation also elicits microscopic morphologic changes, such as glial cell swelling associated with ion and water movement and changes in synaptic vesicle density associated with synaptic transmission. These morphologic changes alter tissue light-scattering, which is considered to be another source of intrinsic signals in the cerebral cortex.[20,45,46] In our recording protocol with infrared observation light, the most plausible source of the optical signals is the stimulus-induced light-scattering changes derived from photoreceptors and surrounding glial cells (e.g., Müller cells[47–49]). That is because (1) strong darkening was observed, even in the foveal center, which lies within a capillary-free zone and is therefore less susceptible to hemoglobin concentration changes,[50] and (2) under infrared light, the contribution of changes in deoxygenated hemoglobin concentration and local blood volume to the optical signal is thought to be much smaller than that of tissue light-scattering.[20]

In this study, we have revealed characteristic response topographies of the retina both in light- and dark-adapted conditions, (1) there was a strong peak of signal intensity in a small area at the foveal center, with a steep decrease away from the fovea in both conditions; (2) the contours of the same signal intensities in the perimacular region were horizontally elongated; and (3) rod-induced signal increased toward the

periphery, forming a circular region with high signal intensity at the same eccentricity of the optic disc. These response patterns were consistent with the results in subjective psychophysical measurements of cone and rod sensitivities,[41-44] and seemed to reflect the current neural activity related to the photoreceptors. As a proof, the spatial property of the optical signals obeyed the several principal features of cone and rod density revealed by macaque and human anatomic studies.[1-4] There are, however, some discrepancies between the response topography and the anatomic distribution of photoreceptors: The dip of the rod ring was not apparent in the horizontal meridian in the response topography, and the crest of the rod ring in the response topography was more peripherally located in superior and temporal retina than that in the anatomic rod density in macaque. These discrepancies may be attributable to the nature of response topography of photoreceptors, which may not completely correspond to their anatomic density distribution; the spatial spread of optical signals, which may deteriorate the fine spatial information; and variability in photoreceptor density distribution among different species or different individuals.[3]

Intrinsic signals can be recorded from the retina noninvasively and more stably than from the cortex. However, there are some potential artifacts that may influence the results. Because of the optical property of the fundus camera system, the intensity of flash stimulus applied to the retina could not be spatially homogeneous, because of the luminance distribution, which has its peak at the center, and the stray light of the flash in the eyeball. In the present system, the light intensity in the central optical axis is theoretically 10% larger than that in the periphery (20° apart from the fovea). In the pilot experiments, we recorded optical signals by adjusting the optical axis of the fundus camera to the foveal center or the peripheral regions apart from the foveal center (10-20°). The difference in the signal intensities of the foveal response in both conditions was as small as the trial-to-trial deviation in each condition, indicating that this problem was not significant in mapping the topography of retinal responsiveness. Opacification in the ocular media, such as corneal edema and vitreous opacity, could also be a cause of the optical artifact.

Eye movement can be another major source of the artifact. Because very small reflectance changes were measured to extract the stimulus-evoked optical response, the location of retinal images before and after stimulus should be completely matched. Slight eye movement during a recording trial causes the quality of the data to deteriorate significantly, which can be corrected by off-line realignment of the retinal images. In the present study, each recording trial was conducted after ensuring that the muscle paralysis was effective enough to stop the eye movements. This artifact, however, could be a serious problem, when we apply it for the clinical examination of alert subjects, who may also produce additional physiological artifacts, such as head movement and change in blood pressure. We are now designing a new recording system to reduce such possible artifacts, and we believe that the trial-to-trial variability could be minimized to that of animal experiments with further mechanical development.

Although lipofuscin autofluoresces,[51] it would be impossible for this to affect our measurement because (1) the first measurements were taken 250 ms after the flash, whereas the excitation of lipofuscin occurs at a much shorter time (<0.1 ms), and (2) if there was continuous illumination, the constant autofluorescence would be deducted, because reflectance records after the flash were subtracted from those before the flash.

There have been many reports in which light reflectance from in vivo retina was measured for evaluating the macular function. Most of them focused on the anatomic distribution of cone photopigment,[33,34] macular pigments,[35,36] and cone mosaic,[5] and a few of them dealt directly with light reflectance changes related to neural activities.[52,53] DeLint et al.[53] pointed out that slower reflectance changes in the fovea during light and dark periods may be linked to cone photoreceptor activity. The results presented by them may be related to the stimulus-evoked light reflectance changes in our study; however, it is difficult to determine, because our technique is different and our measurements are much briefer than their measurements, in which the signal lasts for as long as 15 minutes.

The advantage of this functional measurement of retina is that cone- or rod-induced retinal responsiveness within the posterior pole region can be noninvasively monitored with fine spatial resolution, even from a single trial. There is an urgent need for the development of an objective method to measure retinal function, by which functional disorders can be detected before symptomatic or structural changes occur, especially in adult patients with ARMD or retinitis pigmentosa and in small infants in whom functional examination is always difficult to perform. Although the source of the optical signal is not fully understood, with further technical development, this functional measurement could have a strong potential as a new diagnostic tool for early detection of subtle (subclinical) retinal dysfunction in adults and infants.

Acknowledgments

The authors thank I-han Chou, Hisao Ohde, and Uma Maheswari Rajagopalan for critical comments on the manuscript and Ryota Homma, and Kei Hagiya for technical assistance.

References

1. Osterberg G. Topography of the layer of rods and cones in the human retina. *Acta Ophthalmol.* 1935;13:6-97.
2. Curcio CA, Sloan KR Jr, Packer O, Hendrickson AE, Kalina RE. Distribution of cones in human and monkey retina: individual variability and radial asymmetry. *Science.* 1987;236:579-582.
3. Packer O, Hendrickson AE, Curcio CA. Photoreceptor topography of the retina in the adult pigtail macaque (Macaca nemestrina). *J Comp Neurol.* 1989;288:165-183.
4. Curcio CA, Sloan KR, Kalina RE, Hendrickson AE. Human photoreceptor topography. *J Comp Neurol.* 1990;292:497-523.
5. Roorda A, Williams DR. The arrangement of the three cone classes in the living human eye. *Nature.* 1999;397:520-522.
6. Miyake Y, Shiroyama N, Horiguchi M, Ota I. Asymmetry of focal ERG in human macular region. *Invest Ophthalmol Vis Sci.* 1989; 30:1743-1749.
7. Sutter EE, Tran D. The field topography of ERG components in man. I. The photopic luminance response. *Vision Res.* 1992;32: 433-446.
8. Miyake Y, Horiguchi M, Tomita N, et al. Occult macular dystrophy. *Am J Ophthalmol.* 1996;122:644-653.
9. Riva CE, Falsini B, Logean E. Flicker-evoked responses of human optic nerve head blood flow: luminance versus chromatic modulation. *Invest Ophthalmol Vis Sci.* 2001;42:756-762.
10. Duong TQ, Ngan SC, Ugurbil K, Kim SG. Functional magnetic resonance imaging of the retina. *Invest Ophthalmol Vis Sci.* 2002; 43:1176-1181.
11. Blasdel GG, Salama G. Voltage-sensitive dyes reveal a modular organization in monkey striate cortex. *Nature.* 1986;321:579-585.
12. Grinvald A, Lieke E, Frostig RD, Gilbert CD, Wiesel TN. Functional architecture of cortex revealed by optical imaging of intrinsic signals. *Nature.* 1986;324:361-364.
13. Zepeda A, Arias C, Sengpiel F. Optical imaging of intrinsic signals: recent developments in the methodology and its applications. *J Neurosci Methods.* 2004;136:1-21.
14. Ts'o DY, Frostig RD, Lieke EE, Grinvald A. Functional organization of primate visual cortex revealed by high resolution optical imaging. *Science.* 1990;249:417-420.

15. Frostig RD, Lieke EE, Ts'o DY, Grinvald A. Cortical functional architecture and local coupling between neuronal activity and the microcirculation revealed by in vivo high-resolution optical imaging of intrinsic signals. *Proc Natl Acad Sci USA*. 1990;87:6082-6086.
16. Roe AW, Ts'o DY. Visual topography in primate V2: multiple representation across functional stripes. *J Neurosci*. 1995;15:3689-3715.
17. Ghose GM, Ts'o DY. Form processing modules in primate area V4. *J Neurophysiol*. 1997;77:2191-2196.
18. Malonek D, Tootell RB, Grinvald A. Optical imaging reveals the functional architecture of neurons processing shape and motion in owl monkey area MT. *Proc R Soc Lond B Biol Sci*. 1994;258:109-119.
19. Tsunoda K, Yamane Y, Nishizaki M, Tanifuji M. Complex objects are represented in macaque inferotemporal cortex by the combination of feature columns. *Nat Neurosci*. 2001;4:832-838.
20. Bonhoeffer T, Grinvald A. Optical imaging based on intrinsic signals: the methodology. In: Toga AW, Mazziotta JC, eds. *Brain Mapping*. San Diego: Academic Press; 1996:55-97.
21. Fukuda M, Maheswari RU, Homma R, Matsumoto M, Nishizaki M, Tanifuji M. Localization of activity-dependent changes in blood volume to submillimeter-scale functional domains in cat visual cortex. *Cereb Cortex*. In press.
22. Fox PT, Raichle ME. Stimulus rate dependence of regional cerebral blood flow in human striate cortex, demonstrated by positron emission tomography. *J Neurophysiol*. 1984;51:1109-1120.
23. Fox PT, Miezin FM, Allman JM, Van Essen DC, Raichle ME. Retinotopic organization of human visual cortex mapped with positron-emission tomography. *J Neurosci*. 1987;7:913-922.
24. Ogawa S, Lee TM, Kay AR, Tank DW. Brain magnetic resonance imaging with contrast dependent on blood oxygenation. *Proc Natl Acad Sci USA*. 1990;87:9868-9872.
25. Kwong KK, Belliveau JW, Chesler DA, et al. Dynamic magnetic resonance imaging of human brain activity during primary sensory stimulation. *Proc Natl Acad Sci USA*. 1992;89:5675-5679.
26. Ogawa S, Tank DW, Menon R, et al. Intrinsic signal changes accompanying sensory stimulation: functional brain mapping with magnetic resonance imaging. *Proc Natl Acad Sci USA*. 1992;89:5951-5955.
27. Villringer A, Chance B. Non-invasive optical spectroscopy and imaging of human brain function. *Trends Neurosci*. 1997;20:435-442.
28. Taga G, Asakawa K, Maki A, Konishi Y, Koizumi H. Brain imaging in awake infants by near-infrared optical topography. *Proc Natl Acad Sci USA*. 2003;100:10722-10727.
29. Weliky M, Kandler K, Fitzpatrick D, Katz LC. Patterns of excitation and inhibition evoked by horizontal connections in visual cortex share a common relationship to orientation columns. *Neuron*. 1995;15:541-552.
30. Das A, Gilbert CD. Long-range horizontal connections and their role in cortical reorganization revealed by optical recording of cat primary visual cortex. *Nature*. 1995;375:780-784.
31. Haglund MM, Ojemann GA, Hochman DW. Optical imaging of epileptiform and functional activity in human cerebral cortex. *Nature*. 1992;358:668-671.
32. Toga AW, Cannestra AF, Black KL. The temporal/spatial evolution of optical signals in human cortex. *Cereb Cortex*. 1995;5:561-565.
33. Kilbride PE, Read JS, Fishman GA, Fishman M. Determination of human cone pigment density difference spectra in spatially resolved regions of the fovea. *Vision Res*. 1983;23:1341-1350.
34. Elsner AE, Burns SA, Webb RH. Mapping cone photopigment optical density. *J Opt Soc Am A*. 1993;10:52-58.
35. Kilbride PE, Alexander KR, Fishman M, Fishman GA. Human macular pigment assessed by imaging fundus reflectometry. *Vision Res*. 1989;29:663-674.
36. Elsner AE, Burns SA, Beausencourt E, Weiter JJ. Foveal cone photopigment distribution: small alterations associated with macular pigment distribution. *Invest Ophthalmol Vis Sci*. 1998;39:2394-2404.
37. Bowmaker JK, Dartnall HJ, Mollon JD. Microspectrophotometric demonstration of four classes of photoreceptor in an old world primate, Macaca fascicularis. *J Physiol*. 1980;298:131-143.
38. Bearse MA Jr, Sutter EE. Imaging localized retinal dysfunction with the multifocal electroretinogram. *J Opt Soc Am A*. 1996;13:634-640.
39. Leibu R, Davila E, Zemel E, Bitterman N, Miller B, Perlman I. Development of laser-induced retinal damage in the rabbit. *Graefes Arch Clin Exp Ophthalmol*. 1999;237:991-1000.
40. Bowmaker JK, Dartnall HJ. Visual pigments of rods and cones in a human retina. *J Physiol*. 1980;298:501-511.
41. Mandelbaum J, Sloan LL. Peripheral visual acuity. *Am J Ophthalmol*. 1947;30:581-588.
42. Henson DB. *Visual Fields*. 2nd ed. Oxford: Reed Educational and Professional Publishing; 2000.
43. Birch DG, Herman WK, deFaller JM, Disbrow DT, Birch EE. The relationship between rod perimetric thresholds and full-field rod ERGs in retinitis pigmentosa. *Invest Ophthalmol Vis Sci*. 1987;28:954-965.
44. Pulos E. Changes in rod sensitivity through adulthood. *Invest Ophthalmol Vis Sci*. 1989;30:1738-1742.
45. MacVicar BA, Hochman D. Imaging of synaptically evoked intrinsic optical signals in hippocampal slices. *J Neurosci*. 1991;11:1458-1469.
46. Maheswari RU, Takaoka H, Kadono H, Homma R, Tanifuji M. Novel functional imaging technique from brain surface with optical coherence tomography enabling visualization of depth resolved functional structure in vivo. *J Neurosci Methods*. 2003;124:83-92.
47. Brew H, Attwell D. Electrogenic glutamate uptake is a major current carrier in the membrane of axolotl retinal glial cells. *Nature*. 1987;327:707-709.
48. Newman EA. Voltage-dependent calcium and potassium channels in retinal glial cells. *Nature*. 1985;317:809-811.
49. Reichenbach A, Wohlrab F. Morphometric parameters of Muller (glial) cells dependent on their topographic localization in the nonmyelinated part of the rabbit retina: a consideration of functional aspects of radial glia. *J Neurocytol*. 1986;15:451-459.
50. Weinhaus RS, Burke JM, Delori FC, Snodderly DM. Comparison of fluorescein angiography with microvascular anatomy of macaque retinas. *Exp Eye Res*. 1995;61:1-16.
51. Delori FC, Dorey CK, Staurenghi G, Arend O, Goger DG, Weiter JJ. In vivo fluorescence of the ocular fundus exhibits retinal pigment epithelium lipofuscin characteristics. *Invest Ophthalmol Vis Sci*. 1995;36:718-729.
52. Ripps H, Mehaffey L III, Siegel IM. "Rapid regeneration" in the cat retina: a case for spreading depression. *J Gen Physiol*. 1981;77:335-346.
53. DeLint PJ, Berendschot TT, van de Kraats J, van Norren D. Slow optical changes in human photoreceptors induced by light. *Invest Ophthalmol Vis Sci*. 2000;41:282-289.

技術

網膜における内因性信号計測

角田和繁（つのだかずしげ）
東京医療センター感覚器センター視覚生理学研究室（〒152-8902 東京都目黒区東が丘2-5-1）
E-mail : tsunodakazushige@kankakuki.go.jp

実験のコツと注意点

網膜における内因性信号は大脳皮質における信号よりも一般に大きいが，測定にあたっては特に以下の点に注意する必要がある．

1. 眼球運動をはじめとする生体ノイズの抑制

麻酔下実験においても眼球の微小運動は大きなノイズ源となる．測定時には眼球運動を充分に制御するほか，点眼剤による散瞳，調節麻痺をしっかりと行う．血流の変化も測定に影響するため，心拍数・血圧などの条件を一定に保つように麻酔深度をコントロールする．

2. 可視観察光の影響の排除

視反応にともなう視物質の褪色変化により網膜の反射率は大きく上昇する．これは内因性信号とは逆の極性をもつ信号であるため，観察光としては赤外光を用い，褪色の影響を排除することが重要である．

背景

前号でも紹介された内因性信号による光学計測法は，神経活動にともなって神経組織の光反射率が変化する現象をとらえるもので，実験動物脳での機能的マッピングを行うのに非常に優れた方法である[1-4]．しかし，大脳皮質において光学計測法を行うためには脳表面を露出する必要があり，比較的大きな侵襲を伴うものである．したがってその臨床医学への応用は，てんかん患者に対する脳外科的手術時に行われる実験的なものに過ぎない[5]．一方，ヒトの網膜は内因性信号の計測に有利な特徴をいくつか備えている．まず，眼球の光学系（角膜，水晶体）を通して網膜を直接観察することができ，眼球自体が光学計測における理想的なチェンバーとして働くため，新たにチェンバーを作る手術的な侵襲がない．さらに，網膜外層では視細胞が密に一定方向に並んでいるため，光散乱変化による反射率変化をとらえやすい．

網膜，なかでもその中心に位置する黄斑部は，視力の維持に重要な部位であり，同時に臨床的に様々な疾患が起こりやすい部位でもある．内因性信号計測法が眼底での機能計測に応用できれば，網膜神経機能の客観的な評価法として網膜疾患の早期発見や早期治療につながることが期待される．

我々は内因性信号計測法の臨床応用を目指して，サル眼底における内因性信号計測を行っている（Functional Retinography : FRG）[6]．

脳における測定との相違

ヒトおよびサルの眼底は**図1a**に示すような特殊な解剖学的構造をしている．我々は測定を行う際に，眼底を中心窩網膜・周辺部網膜・視神経乳頭部の3部位に分類している．中心窩は錐体視細胞が密集している領域で毛細血管が存在しない（**図1b**）．周辺部網膜は典型的な10層構造をしており，杆体および錐体視細胞の他，双極細胞，神経節細胞，グリア細胞および網

1344-0128/06/¥100/頁/JCLS

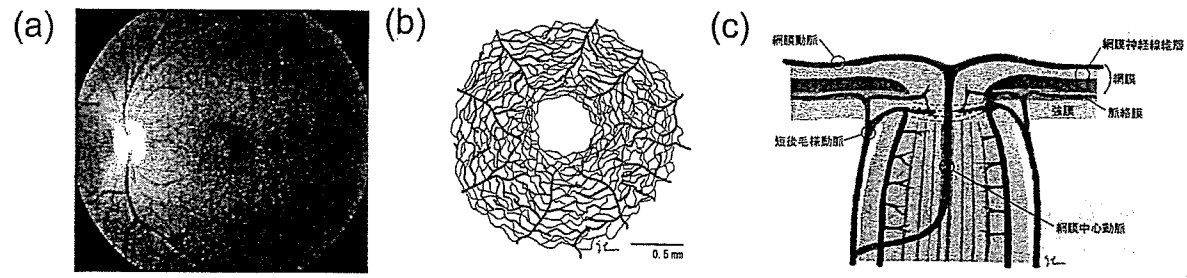

図1　眼底の構造

a：アカゲサルの眼底写真．b：中心窩毛細血管網の模式図．網膜中心部（300～500 μm）は無血管領域であり，錐体視細胞が密集している．c：視神経乳頭部の垂直断面模式図．ここには視細胞は存在せず，中心動静脈のほか毛細血管が豊富に存在する．(p.8，カラー図参照)

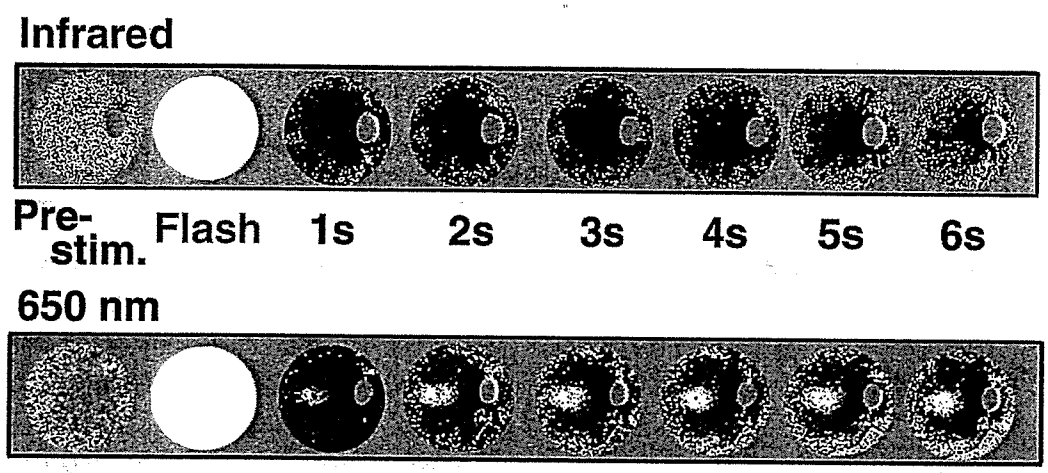

図2　赤外および可視観察光による内因性信号の違い

上段：赤外光観察下におけるフラッシュ刺激後の網膜反射率変化．網膜面全体の反射率低下（暗くなる変化）が見られる．下段：650 nmの観察光での網膜反射率変化．錐体視細胞の多い黄斑部付近では，視細胞の褪色変化により反射率が増加している（明るくなる変化）．

膜血管などが存在する．視神経乳頭部は神経節細胞の軸索の束であり，視細胞は存在しないが血管は豊富である（図1c）．これら3つの部位で記録される内因性信号は，それぞれ異なる信号起源を持っていると考えられる．

脳における内因性信号測定と最も異なる点は，受容体そのものが測定の対象である，ということである．すなわち刺激光のみならず観察光が内因性信号を惹起する可能性がある．また網膜固有の変化として，視細胞の褪色変化があげられる．褪色変化とは，光刺激によって視物質の異性化が起こるさい，視物質の光吸収特性が変化することである．吸収率のピークはより短波長側にシフトし，その結果光反射率の増加が観察される．これは内因性信号とは極性の異なる変化であり，観察光が可視光の場合は内因性信号と褪色変化という，2つの信号の和を計測していることになる（図2）[7,8]．このため神経活動のマッピングを行うさいには，観察光として近赤外光を用いる必要がある．

実験方法

我々の施設で行っている標準的な実験方法について以下に述べる[6]．

1. 実験動物

全身麻酔下のアカゲサルおよびニホンザルを用いて

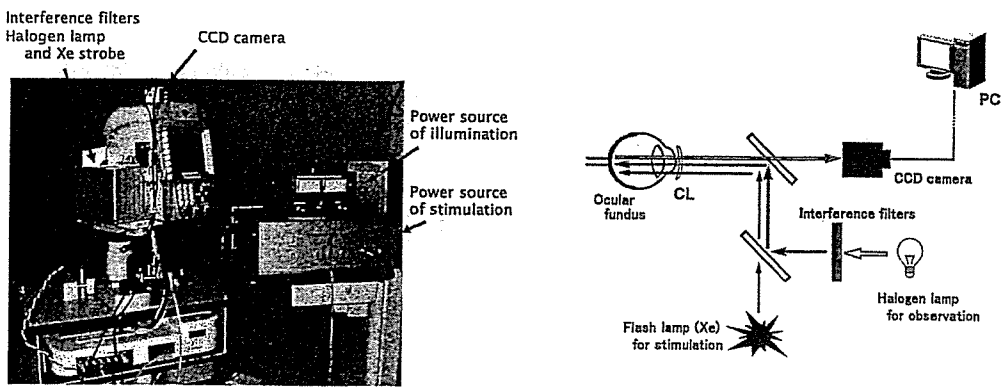

図3　網膜内因性信号計測システム（FRG）
左：計測装置の外観．右：実験セットアップの模式図．

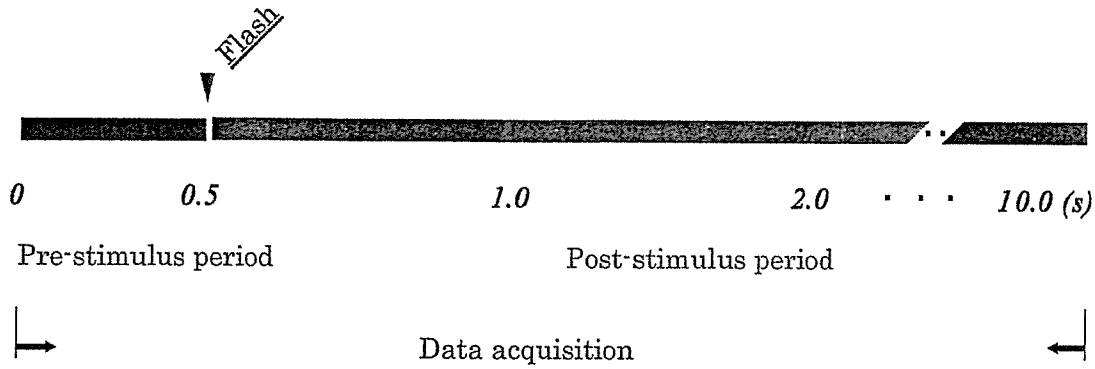

図4　測定開始からのタイムテーブル

いる．麻酔の導入には硫酸アトロピン（0.08 mg/kg），ドロペリドール（0.25 mg/kg）および塩酸ケタミン（5.0 mg/kg）の筋注を用いる．気管挿管後，筋弛緩剤として臭化ベクロニウムを持続静注（0.4～0.5 mg/kg/hr）し，笑気およびイソフルラン（1.0％）による吸入麻酔を行っている．散瞳，調節麻痺のため，トロピカミド・塩酸フェニレフリンの点眼を2時間おきに行う．

2. 測定システム

網膜反射率の計測には，市販されている眼底カメラの光学系，投光系を改良し，光刺激装置およびCCDカメラを付け加えたものを用いる（図3）．眼底観察用のハロゲン光は，干渉フィルター（800～900 nm）を透過して眼底後極部を照明する．解像度640×480，毎秒30フレームのCCDカメラによって眼底からの光反射率変化を持続的に記録する．測定開始から0.5秒後に眼底後極部全体を白色キセノンフラッシュ（1 ms）にて刺激する（図4）．一回の測定は通常5～10秒間行う．呼吸に伴う反射率変化の影響を減らすため，測定時には一時的に人工呼吸器を停止させている．

3. 内因性信号の計算方法

刺激前0.5秒間の平均画像の反射率と，刺激後の画像における反射率との比をピクセル毎に計算し，その比を256階調にスケーリングし画像化する．大脳皮質での測定では通常10～30回ほどの平均加算を要するが，網膜においては加算平均を行わないsingle trialでのマッピングが可能である．

III　実際の測定結果

フラッシュによるびまん性刺激によって視細胞が活動すると，網膜全体の反射率が低下し画像上暗く描出される（図5）．この内因性信号は中心窩で最も強い．信号強度を疑似カラーで表示すると，明順応下では中

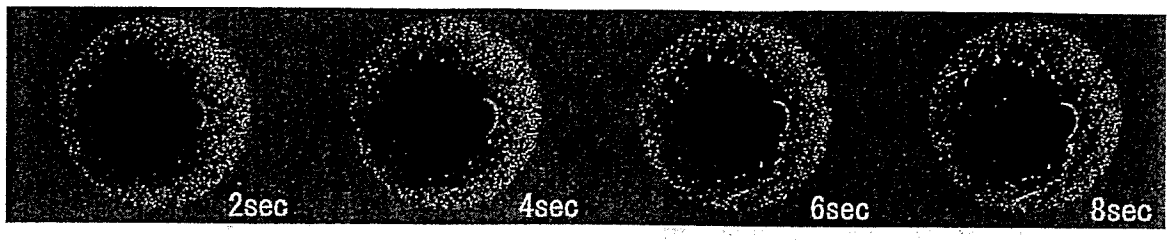

図5　赤外光観察下（800～900 nm）における網膜内因性信号

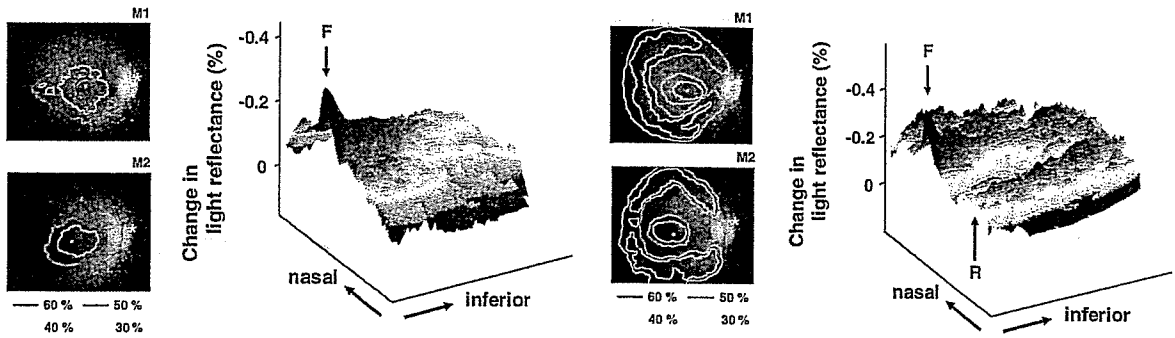

図6　網膜内因性信号のトポグラフィー

左図は明順応下，右図は暗順応下における記録．（白点は中心窩，＊印は視神経乳頭部を表す）

（p.8，カラー図参照）

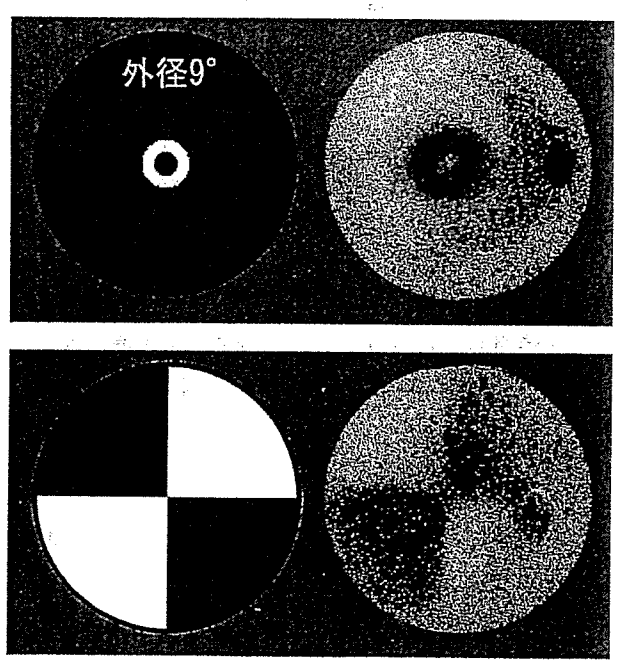

フラッシュ刺激の形状　　内因性信号

図7　刺激部位に対応した，網膜局所の内因性信号

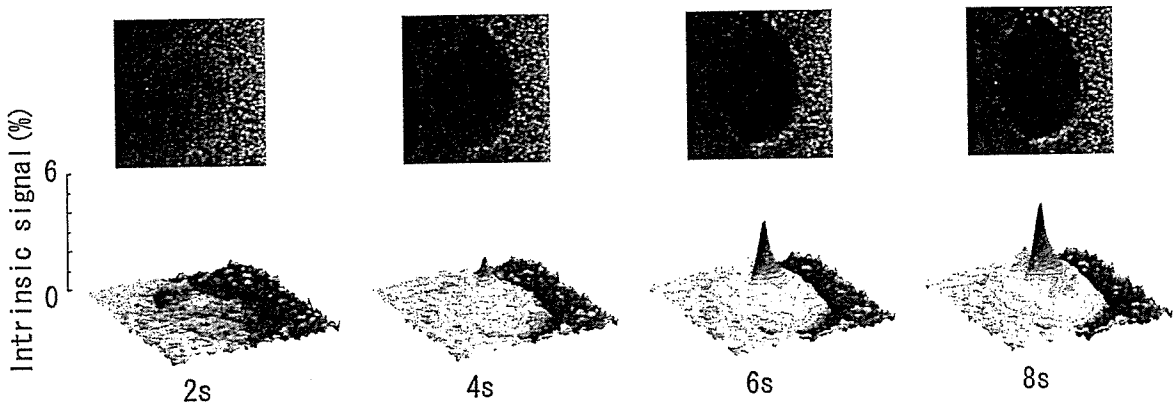

図8　視神経乳頭部におけるフラッシュ刺激後の内因性信号変化（上）および同部位のトポグラフィー（下）
（p.8，カラー図参照）

心窩に内因性信号の急峻なピークを認め，周辺部に向かって減少するが，暗順応下では中心窩に加えて周辺部にドーナツ状のピークを認める（図6）．内因性信号のピークは中心窩では錐体視細胞，周辺部では杆体視細胞の解剖学的な分布によく一致しており，網膜内因性信号の発生には視細胞が寄与していると思われる[9,10]．

また，網膜との共役面にフィルターを置いて局所フラッシュ刺激を行うと，刺激部位に相当する網膜のみから内因性信号を記録することができる（図7）．

一方，視神経乳頭部に注目すると，ここでは網膜面とは異なりフラッシュ刺激後にゆっくりと信号が強くなっていく（図8）．これは刺激後の血流増加を反映した光散乱強度変化と考えられ，中心動静脈に相当する視神経乳頭中央部に急峻なピークが見られる[11]．

まとめ

網膜における内因性信号の測定方法と実際の測定結果について簡単に説明した．測定にあたっては二つの画像の差を用いるため画像の偏位（眼球運動），光量の変化（瞳孔反応・光の入り具合）等様々な要因が障害となりうる．現在のところ，ヒト網膜において詳細なマッピングを行うまでには至っていない．今後，測定技術および解析方法等の改良により客観的網膜機能イメージング法としての臨床応用が可能となれば，さまざまな網膜疾患の早期発見・早期治療に役立つものと確信している．

参考文献

1) Grinvald A, et al : Functional architecture of cortex revealed by optical imaging of intrinsic signals. Nature **324** : 361-364, 1986.
2) Bonhoeffer T, Grinvald A : Optical Imaging Based on Intrinsic Singals: The Methodology. In: Toga AW, Mazziotta JC, eds. Brain Mapping. San Diego: Academin Press; 55-97, 1996.
3) Tsunoda K, et al : Complex objects are represented in macaque inferotemporal cortex by the combination of feature columns. Nat Neurosci **4** : 832-838, 2001.
4) Fukuda M, et al : Localization of activity-dependent changes in blood volume to submillimeter-scale functional domains in cat visual cortex. Cereb Cortex **15** : 823-833, 2005.
5) Haglund MM, et al : Optical imaging of epileptiform and functional activity in human cerebral cortex. Nature **358** : 668-671, 1992.
6) Tsunoda K, et al : Mapping Cone- and Rod-Induced Retinal Responsiveness in Macaque Retina by Optical Imaging. Invest. Ophthalmol **45** : 3820-3826, 2004.
7) Kilbride PE, et al : Determination of human cone pigment density difference spectra in spatially resolved regions of the fovea. Vision Res **23** : 1341-1350, 1983.
8) Elsner AE, et al : Mapping cone photopigment optical density. J Opt Soc Am A **10** : 52-58, 1993.
9) Osterberg G : Topography of the layer of rods and cones in the human retina. Acta ophthalmol **13** : 6-9, 1935.
10) Curcio CA, et al : Distribution of cones in human and monkey retina: individual variability and radial asymmetry. Science. **236** : 579-582, 1987.
11) Riva CE, et al : Flicker-evoked responses of human optic nerve head blood flow: luminance versus chromatic modulation. Invest Ophthalmol **42** : 756-762, 2001.

J Neurophysiol 96: 3147–3156, 2006.
First published August 30, 2006; doi:10.1152/jn.01224.2005.

Representation of the Spatial Relationship Among Object Parts by Neurons in Macaque Inferotemporal Cortex

Yukako Yamane,[1,2] Kazushige Tsunoda,[1,3] Madoka Matsumoto,[1] Adam N. Phillips,[1] and Manabu Tanifuji[1]
[1]*Laboratory for Integrative Neural Systems, RIKEN Brain Science Institute, Saitama;* [2]*Division of Biological Sciences, Graduate School of Science, Hokkaido University, Sapporo;* [3]*Laboratory of Visual Physiology, National Institute of Sensory Organs, Tokyo, Japan*

Submitted 21 November 2005; accepted in final form 27 August 2006

Yamane, Yukako, Kazushige Tsunoda, Madoka Matsumoto, Adam N. Phillips, and Manabu Tanifuji. Representation of the spatial relationship among object parts by neurons in macaque inferotemporal cortex. *J Neurophysiol* 96: 3147–3156, 2006. First published August 30, 2006; doi:10.1152/jn.01224.2005. We investigated object representation in area TE, the anterior part of monkey inferotemporal (IT) cortex, with a combination of optical and extracellular recordings in anesthetized monkeys. We found neurons that respond to visual stimuli composed of naturally distinguishable parts. These neurons were sensitive to a particular spatial arrangement of parts but less sensitive to differences in local features within individual parts. Thus these neurons were activated when arbitrary local features were arranged in a particular spatial configuration, suggesting that they may be responsible for representing the spatial configuration of object images. Previously it has been reported that many neurons in area TE respond to visual features less complex than natural objects, but it has remained unclear whether these features are related to local features of object images or to more global features. These results indicate that TE neurons represent not only local features but also global features such as the spatial relationship among object parts.

INTRODUCTION

Visual information about object images is conveyed from early visual area V1 to inferior temporal (IT) cortex through areas V2 and V4 in macaque monkeys (for review, see Logothetis and Sheinberg 1996). Area TE is a ventral part of IT cortex and is the site that represents object images necessary for visual recognition (Gross 1994; Logothetis and Sheinberg 1996).

Early studies on visual responses of TE neurons showed that these neurons respond to various visual stimuli including natural object images (Bruce et al. 1981; Desimone et al. 1984; Gross et al. 1979; Perrett et al. 1982; Schwartz et al. 1983). More recently, a number of studies have attempted to identify the simplest visual features that activate individual neurons in area TE (Kobatake and Tanaka 1994; Tanaka et al. 1991). These studies have revealed that essential stimuli for TE neurons are visual features that are geometrically less complex than natural objects. Thus combinations of visual features are necessary for neural representation unique to individual object images in area TE.

As in the primary visual cortex, neurons in area TE with similar response properties are reported to be clustered into columns (Fujita et al. 1992; Gochin et al. 1991). The columns responding to visual stimuli have been visualized with intrinsic signal imaging as darkened spots scattered across the cortical surface (Tsunoda et al. 2001; Wang et al. 1996, 1998). In particular, Tsunoda and colleagues used this technique together with conventional extracellular recordings and showed that an object image activates multiple spots, each of which represents a particular visual feature of the object image (Tsunoda et al. 2001). They reported that some of the visual features represented by activated spots were local features of object images, that is, features that appear in a spatially localized part of the object image. Thus it remains unknown how spatial arrangements of these local features in an object image are specified. Neurons in area TE may represent global features, such as spatial configuration of local features, in addition to spatially localized features. In this paper, we address this question by combining data from intrinsic signal imaging and extracellular recordings.

METHODS

Anesthesia and the general recording condition

Four rhesus monkeys were artificially ventilated with a mixture of N_2O, O_2, and isoflurane for anesthesia and paralyzed with pancuronium bromide or vecuronium bromide (Tsunoda et al. 2001). The visual stimuli were presented on a 20-in CRT display placed 57 cm from the eye contralateral to the recording hemisphere. The pupil of the eye was dilated by local application of 0.5% tropicamide 0.5% phenylephrine, and the cornea was covered with a contact lens of appropriate power to focus the visual stimuli onto the retina. The fovea was identified with a custom-made ophthalmoscope, and the position of the fovea was back-projected onto the center of the CRT screen. Except for three-dimensional (3D) objects for manual presentations, the visual stimuli were presented at the center of the CRT display. Electroencephalography (EEG), electrocardiography (ECG), expired CO_2 concentration, and rectal temperature were monitored throughout the experiments. The experimental protocol was approved by the Experimental Animal Committee of the RIKEN Institute. All experimental procedures were done in accordance with the guidelines of the RIKEN Institute and the National Institute of Health.

Intrinsic signal imaging

The dorsal part of area TE was exposed and illuminated by light with a wavelength of 605 nm through a glass cover slip window attached to a titanium chamber centered 15.0–17.5 mm anterior to the ear bar position (Tsunoda et al. 2001). Reflected light from the cortex was detected by a low-noise video camera (frame rate, 1/30 frames/s; S/N ratio, 60 dB; CS8310, Teli, Japan) and digitized by a 10-bit video capture board (Pulsar, Matrox). The light was focused to a depth of 500 μm below the cortical surface. The imaged area was 6.5 × 4.9

Address for reprint requests and other correspondence: M. Tanifuji, Laboratory for Integrative Neural Systems, RIKEN Brain Science Institute, 2-1 Hirosawa, Wako-shi, Saitama 351-0198, Japan (E-mail: tanifuji@riken.jp).

The costs of publication of this article were defrayed in part by the payment of page charges. The article must therefore be hereby marked "*advertisement*" in accordance with 18 U.S.C. Section 1734 solely to indicate this fact.